COMPDYN 2015
5th ECCOMAS Thematic Conference on
Computational Methods in Structural Dynamics and Earthquake Engineering
M. Papadrakakis, V. Papadopoulos, V. Plevris (eds.)
Crete Island, Greece, 25–27 May 2015

ASSESSMENT OF STONE MASONRY WALLS WITH DETERIORATION AT THEIR BASE USING NON-LINEAR FINITE ELEMENT ANALYSES

Georgios Papadopoulos, Dimos C. Charmpis and Rogiros Illampas

Department of Civil and Environmental Engineering, University of Cyprus,
75 Kallipoleos Str., P.O. Box 20537, 1678 Nicosia, Cyprus,
E-mails: giwrgospapadopoulos35@gmail.com, charmpis@ucy.ac.cy, rilamp01@ucy.ac.cy

Keywords: Structural safety, local failure, damage tolerance, damage scenario, non-linear finite element analysis, notional material removal, progressive collapse.

Abstract. *Masonry walls are exposed to various potentially damaging factors, which arise due to common environmental effects or accidental actions. Local damage on a masonry wall operating as a primary load carrying component may trigger partial or full collapse of the wall and of the structural system it is supporting. Therefore, reliably assessing (potentially) damaged masonry walls is a crucial aspect in maintaining the desired safety level and decide the appropriate retrofit measures possibly required.*
In the present work, the influence of deterioration at the base of stone masonry walls on their structural response is investigated. For this purpose, plane stress non-linear Finite Element (FE) analyses are performed for various wall configurations and base deterioration scenarios. Hence, the in-plane lateral strength is computed for walls, which are artificially damaged by notionally removing masonry material from the walls' base. By comparing the remaining carrying capacity of a 'damaged' wall with the carrying capacity of the corresponding intact wall, the structural damage tolerance of the deteriorated wall can be quantitatively assessed. The results obtained demonstrate the effects of base deterioration on the lateral resistance of stone masonry walls and facilitate the decision making process for a possible small- or large-scale intervention.

1 INTRODUCTION

Stone masonry walls operating as primary load carrying components are encountered in several historic/traditional as well as contemporary structures. As any structural component, such walls are exposed to various potentially damaging factors, which arise due to common everyday or frequent environmental effects, as well as infrequent severe/accidental actions [1-5]. Local damage may trigger partial or full collapse of a masonry wall and of the structural system it is supporting. Therefore, the understanding of the structural behaviour and the estimation of the remaining carrying capacity of a damaged masonry wall are crucial aspects in its assessment with respect to the safety level provided and the retrofit measures possibly required.

Typically, the part most prone to deterioration is the base of the masonry wall. Hence, the present work is concerned with the influence of deterioration at the base of stone masonry walls on their structural response. Base deterioration develops primarily due to rising damp, which penetrates into the wall and then evaporates causing disintegration of the wall constituents (stone/mortar). This deterioration process starts from the foundation level, at the external wall surface, and proceeds upwards and inwards, undercutting this way the wall structure. Depending on the extent of deterioration, possible interventions may aim at eliminating or at least diminishing the impacts of the deterioration factor (e.g. reduce damp by installing more effective drainage system) and/or at repairing/strengthening the damaged wall (e.g. through stone/mortar replacement or injection grouting).

In this work, plane stress non-linear Finite Element (FE) analyses are performed to examine the in-plane lateral resistance of stone masonry walls under various base deterioration scenarios. The length of the masonry walls considered is 6m, the height is 3m and the thickness is 50cm, while various configurations of door/window openings are assumed. For each case investigated, the intact (non-deteriorated) wall is first analysed. Then, several base deterioration scenarios are defined through the notional thickness reduction of certain elements of the wall FE mesh. The results obtained for the FE models with notionally removed masonry material allow the estimation of the structural damage tolerance of the deteriorated wall. Such results can greatly assist in establishing rational damage control and retrofit strategies for masonry walls with deterioration at their base.

The remainder of this paper is organized as follows. Section 2 provides the geometrical characteristics of the masonry walls analysed in the present work. Section 3 describes the base deterioration scenarios assumed for the analysed masonry walls. Section 4 presents the way the walls are simulated using non-linear FE analysis. FE simulation results are reported in section 5. Finally, the conclusions of the paper are given in section 6.

2 GEOMETRICAL CHARACTERISTICS OF ANALYSED MASONRY WALLS

Four different stone masonry wall configurations are examined in this work (Fig. 1). In all 4 configurations, the same basic geometrical wall characteristics are assumed: 6m×3m×50cm (length×height×thickness of the wall). The difference in these configurations is made by the presence of window/door openings. Hence, the 4 configurations correspond to: (a) a wall without openings, (b) a wall with a central window opening, (c) a wall with a central door opening and (d) a wall with a door and a window opening. Window openings have dimensions 1m×1m, while door openings have dimensions 1m×2m (width×height). Timber lintels are assumed to be installed above all openings. The detailed geometrical characteristics for the 4 wall configurations are given in Fig. 1.

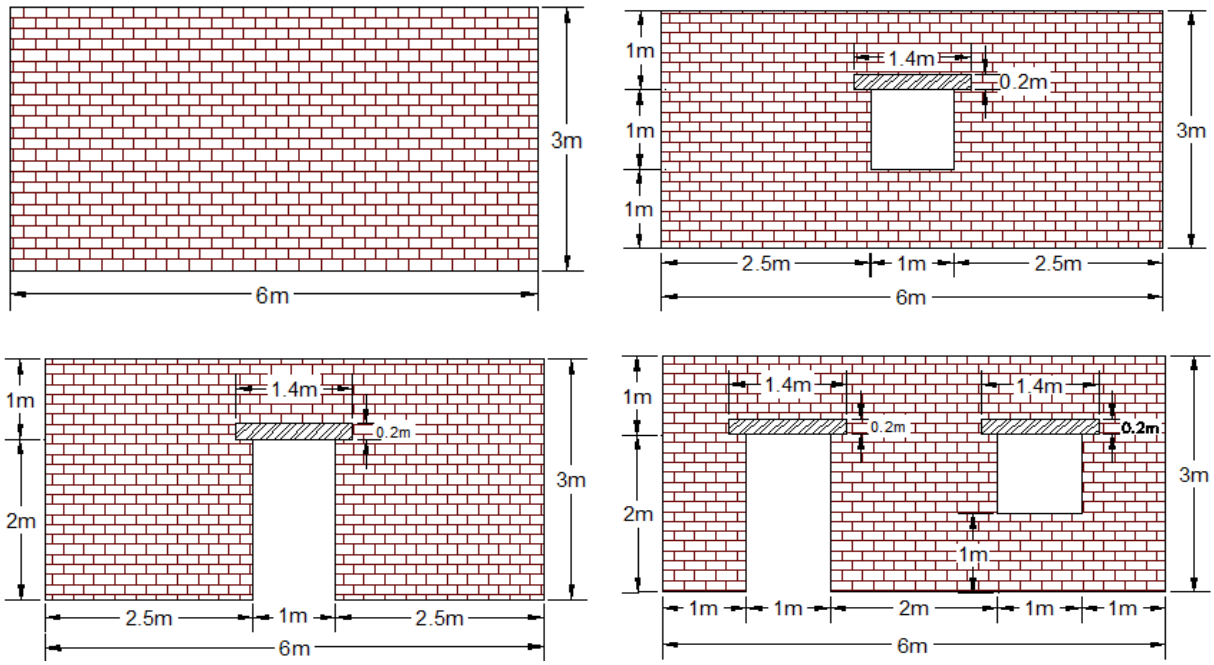

Figure 1: Geometrical characteristics of analysed masonry walls.

3 ARTIFICIAL DETERIORATION THROUGH NOTIONAL MATERIAL REMOVAL

In the present work, deterioration is simulated by the notional material removal from the base of a wall. It is assumed that deterioration develops uniformly over the wall's length. Hence, 3 longitudinal deterioration zones are defined, as shown in Fig. 2; the height of zone 1 is 10cm, while the height of each of zones 2 and 3 is 20cm. Masonry material is notionally removed from the 'deteriorated' wall region (i.e. from the 3 deterioration zones) in 15 phases, as described in Table 1. In each phase, the masonry material removed from a zone has a constant thickness 0-25cm within this zone, i.e. the deterioration thickness is constant over the length and height of a zone. At any phase, each zone may have a different deterioration thickness, however the deterioration thickness in a lower zone is always larger or equal to the one of a higher zone. The maximum height of the 'deteriorated' wall region is 50cm, which is encountered when all 3 zones have non-zero deterioration thicknesses. Characteristic deterioration phases are illustrated in Fig. 3.

Each of the 15 material removal phases defined corresponds to a deterioration scenario of the masonry wall. A FE analysis is conducted to determine the load carrying capacity of the wall for each deterioration scenario. Through the 'gradual' material removal in phases and the FE analysis in each phase, we can monitor the wall's structural behaviour for deterioration effects of increasing severity.

In order to facilitate the reference to deterioration phases, a deterioration index I_{det} is defined, which quantitatively describes the extent of artificial deterioration assumed. Referring to the rectangular cross-section 50cm×300cm (thickness×height) of the masonry wall, we concentrate on its lowest square of 50cm×50cm, which includes the 3 deterioration zones mentioned earlier; this base part of the wall has a cross-sectional area A_b=2500cm^2. Hence, the deterioration index is expressed as:

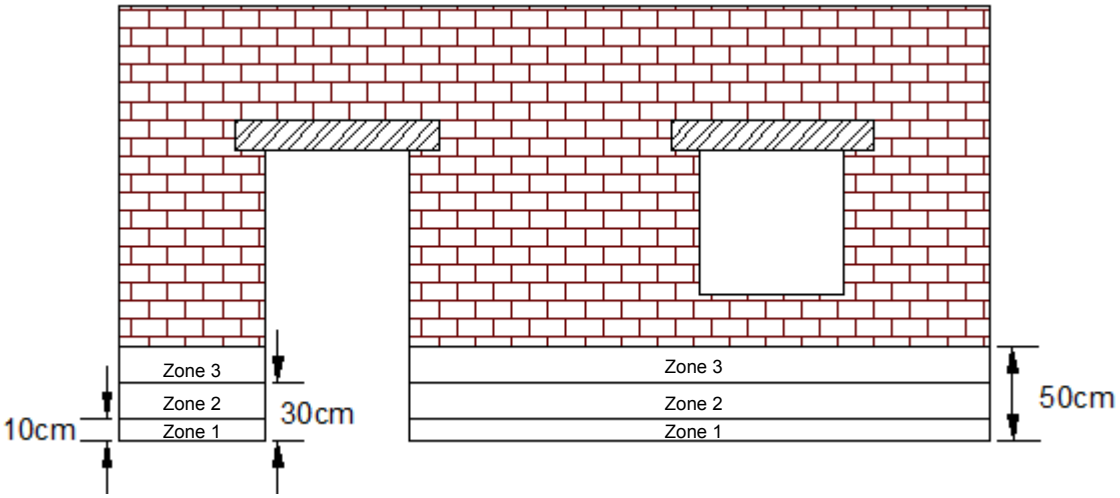

Figure 2: Side view of typical masonry wall showing the 3 longitudinal deterioration zones at the base.

Deterioration phase	I_{det}	Deterioration thickness [cm]		
		Zone 1	Zone 2	Zone 3
0	0.00	0	0	0
1	0.02	5	0	0
2	0.04	10	0	0
3	0.08	10	5	0
4	0.12	10	10	0
5	0.14	15	10	0
6	0.18	15	15	0
7	0.22	15	15	5
8	0.26	15	15	10
9	0.30	15	15	15
10	0.32	20	15	15
11	0.36	20	20	15
12	0.40	20	20	20
13	0.42	25	20	20
14	0.46	25	25	20
15	0.50	25	25	25

Table 1: Definition of deterioration phases.

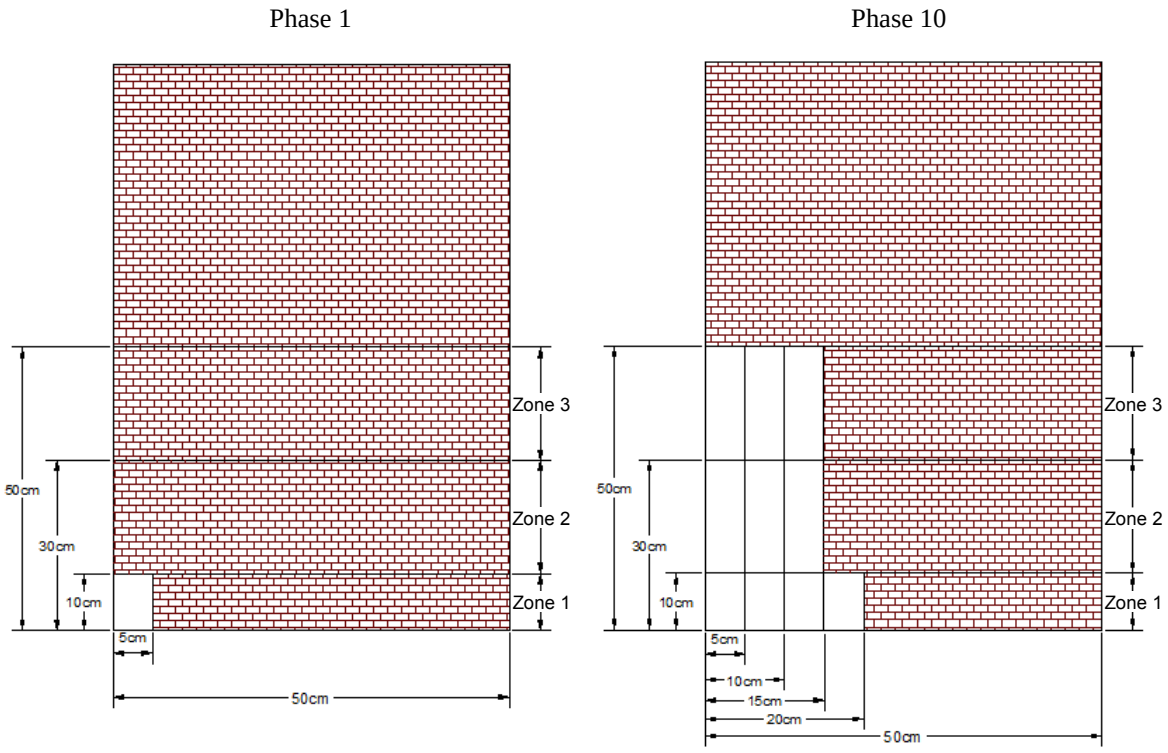

Figure 3: Cross-sectional view at the base of a masonry wall – illustration of characteristic deterioration phases.

$$I_{det} = \frac{A_{b,det}}{A_b}, \tag{1}$$

where $A_{b,det}$ is the cross-sectional area of the wall, which is notionally removed to simulate the masonry material lost due to base deterioration. For example, in deterioration phase 10 (Fig. 3), the removed wall material has a cross-sectional area $A_{b,det}$=20cm×10cm+15cm×40cm=800cm^2, which yields a deterioration index I_{det}=800/2500=0.32. Thus, I_{det} expresses the reduction of the effective load-bearing section at the base of the wall and takes values between 0 (no deterioration – phase 0) and 0.5 (maximum deterioration – phase 15). Table 1 gives the indexes I_{det} for all deterioration phases considered.

4 FINITE ELEMENT MODELLING AND ANALYSIS OF MASONRY WALLS

Various analysis and assessment approaches for masonry structures can be found in the literature (e.g. [6]). In the present work, computational analysis of the in-plane response of masonry wall configurations is conducted with Abaqus/CAE [7] using plane stress FE continuum models (Fig. 4). In the numerical models examined, both the masonry walls and the openings' timber lintels, which are commonly incorporated in traditional constructions, are represented. All bodies are discretized into structured meshes composed of 4-noded 2D bilinear plane stress quadrilateral elements with reduced integration and hourglass control (CPS4R). The plane stress thickness of the undamaged masonry elements and of the lintels is defined as 50cm. Depending on the damage pattern examined, different plane stress thicknesses are assigned to areas of the masonry subjected to deterioration.

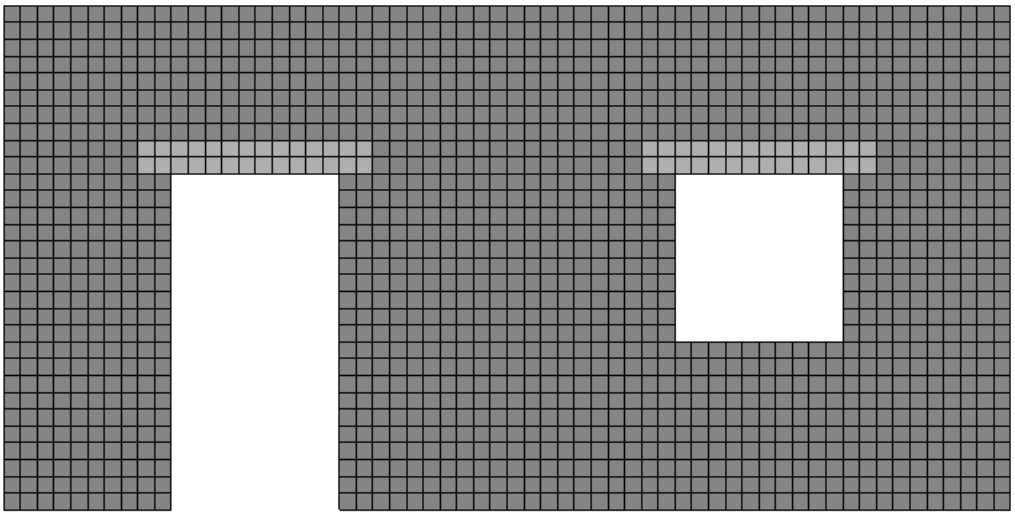

Figure 4. Side view of typical masonry wall and its FE mesh.

Masonry is numerically handled in the context of a macro-modelling strategy. The masonry constituents (i.e. the units, mortar and the unit-mortar interfaces) are hence smeared out into a fictitious homogeneous continuum represented by a FE mesh. The behaviour of the homogenized masonry medium is simulated using the damaged plasticity constitutive model [8], which has been successfully used in FE analyses of masonry structures [9,10]. The adopted model uses brittle fracture concepts in combination with scalar (isotropic) damage plasticity to represent the inelastic response of a material. Two principal damage mechanisms are assumed: tensile cracking and compressive crushing.

The modelling parameters used for the formulation of the constitutive law are based on relevant experimental data reported in the literature. Density is specified as ρ=2500kg/m^3 according to the properties assessed in [11] and the parameters used in [12] for the simulation of stone masonry structures. The elastic modulus and Poisson's ratio are defined as E=3000MPa and v=0.15, respectively, in line with the information given in [13] and [14] for single-leaf calcarenite stone masonry walls and the range of experimental results summarized in [15].

Under uniaxial compression, initial yielding is assumed to be followed by hardening behaviour up to the maximum allowable stress. After the ultimate strength is attained, stress softening is assumed to develop. Compressive response is specified by expressing compressive stresses as a function of plastic (crushing) strains (Fig. 5(a)). For this purpose, the polynomial stress-strain relation developed in [16] for tuff masonry is adopted:

$$\bar{\sigma}_c = \begin{cases} -0.7144\bar{\varepsilon}_c^3 + 0.4549\bar{\varepsilon}_c^2 + 1.2595\bar{\varepsilon}_c & \text{for } 0 \le \bar{\varepsilon}_c \le 1.12 \\ -0.0107\bar{\varepsilon}_c^3 + 0.1388\bar{\varepsilon}_c^2 - 0.6487\bar{\varepsilon}_c + 1.545 & \text{for } 1.12 \le \bar{\varepsilon}_c \le 4 \end{cases} \quad (2)$$

In the above equation, $\bar{\sigma}_c$ and $\bar{\varepsilon}_c$ are normalized values obtained by dividing the stress with the compressive strength ($\bar{\sigma}_c = \sigma / f_c$) and the axial deformation with the strain at peak stress ($\bar{\varepsilon}_c = \varepsilon / \varepsilon_c$). A stress-strain expression analogous to (2) has been derived in [17] for adobe masonry. Material non-linearity in compression is considered to initiate at stresses exceeding 30% of the bearing capacity. Compressive strength is set as f_c=2MPa based on the data quoted in [16], while strain at peak compressive strength is computed as ε_c=0.00094mm/mm after solving Eq. (2).

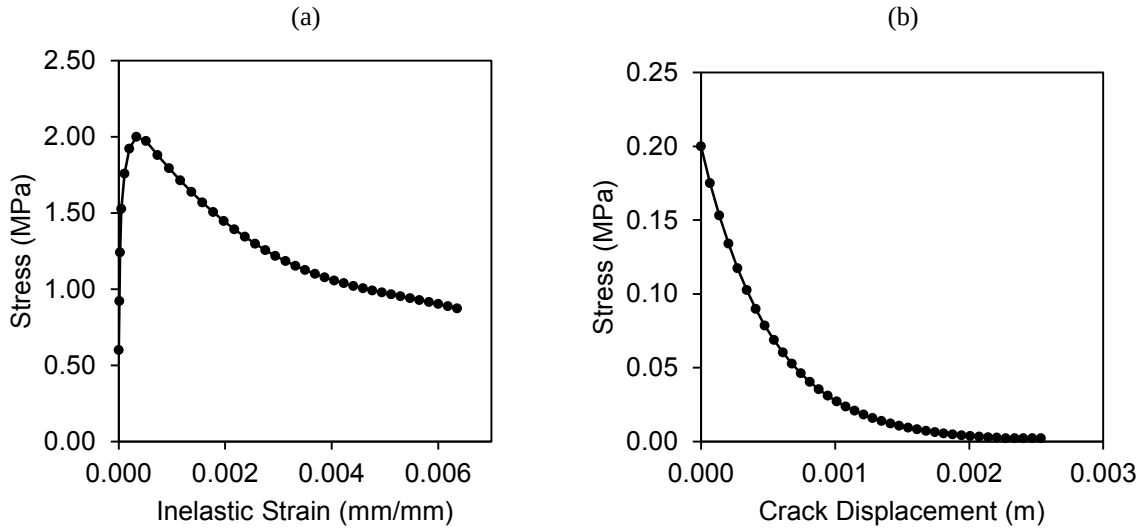

Figure 5: Compressive stress-plastic strain and tensile stress-crack displacement input data specified for the homogenized stone masonry medium in compression (a) and tension (b), respectively.

Under uniaxial tension, masonry's behavior is presumed to be linearly elastic up to the point where the failure stress is reached. Beyond the failure stress, softening stress-strain response is specified using the exponential model proposed in [18]:

$$\sigma_t = f_t \exp\left(-\frac{h f_t}{G_f}\varepsilon_t^{ck}\right). \tag{3}$$

In equation (3), f_t is the tensile strength of the masonry, assumed equal to 10% of the compressive strength, G_f is the tensile fracture energy, selected as G_f=100N/m [19], ε_t^{ck} is the tensile cracking strain and h is the characteristic crack length that is estimated from the elements' average dimensions (h_x, h_y) as $h = \sqrt{2h_x h_y}$ [20]. The global size of the masonry elements' sides is set as h_x=h_y=10±1cm, in order to satisfy the energy criterion associated with the tension softening model used:

$$h \le \frac{G_f E}{f_t^2}. \tag{4}$$

Softening behaviour is assigned by converting tensile plastic strains to equivalent cracking displacements using the elements' characteristic crack length and by specifying stress-cracking displacement tabular data (Fig. 5(b)).

The complete description of the yield surface, in addition to the above, requires the definition of four plasticity parameters. Default values suggested in [7] for concrete and cement-based materials are hereby adopted. The rate at which the hyperbolic flow potential approaches its asymptote is set as e=0.1. The ratio between the initial equibiaxial and the initial uniaxial compressive yield stresses is defined as σ_{b0}/σ_{c0}=1.16. Parameter K_c that affects the shape of the yield surface in the deviatoric plane is set equal to 0.67. Based on [21], a value of ψ=12º is specified for the dilation angle controlling the plastic volumetric strain developed upon plastic shearing.

The timber lintels of the masonry structures examined are modelled to exhibit linearly elastic and isotropic behaviour. The material parameters used are also drawn from the literature [22,23] and are as follows: density ρ=670kg/m^3; Young's modulus E=7000MPa; Poisson's ratio v=0.3.

Perfect bonding is assumed to exist between the timber members and the walls. Therefore, common nodes are assigned at the areas where the lintels are in contact with the masonry. The walls' base is considered to be pinned and hence translational degrees of freedom in the x- and y-directions are constrained.

As regards gravitational loads, the self-weight of each wall analysed is taken into account, as well as a dead load corresponding to a 20cm thick concrete slab supported by the wall; moreover, a live load of 2kN/m^2 is applied. The wall is also subjected to a horizontal seismic load, which is simulated as a lateral displacement enforced at the top of the wall. Specifically, a lateral displacement of up to 5mm is incrementally imposed at each top node of the wall.

Each FE analysis is conducted in two phases: first, the gravitational (dead and live) loads are applied in up to 100 increments; then, the lateral displacements are imposed in up to 1000 increments at the wall's top nodes. Both phases are performed using a general non-linear static procedure with automatic stabilization employing the full Newton solution scheme. The effects of geometric non-linearities are taken into account in both analysis phases.

5 FINITE ELEMENT SIMULATION RESULTS

The main structural response quantity monitored during a masonry wall's FE simulation is the base shear developed due to the lateral top displacement imposed. The base shear is calculated by summing the lateral reactions developed at all base nodes of the wall, which are pinned. Thus, force-displacement curves are constructed, which describe the relation between the incrementally enforced lateral displacement and the corresponding base shear developed. The maximum base shear observed at any instance of the FE analysis represents the lateral in-plane strength (carrying capacity) of the masonry wall analysed.

Figure 6 presents the force-displacement curves derived by the FE analyses performed for the 4 masonry wall configurations without removed material to simulate base deterioration. The 4 curves have similar highly non-linear shapes, which are typical in masonry structural analysis: a non-linear ascending branch is followed by a post-peak softening branch. In all 4 intact walls, the maximum base shear is attained for a lateral top displacement of 1.0-1.5mm, while a significant residual carrying capacity is observed at the end of the FE analysis (at lateral top displacement of 5mm). It is noted that, in all other FE analyses conducted with assumed base deterioration, force-displacement curves have shapes that are similar to the ones depicted in Fig. 6.

The effect of openings on the intact wall's lateral strength is evident in Fig. 6. The maximum base shear for the wall without openings is 473kN; for the walls with openings, it reduces to 370kN (window opening), 326kN (door opening) and 311kN (door and window openings). The 4 configurations exhibit differences also in terms of the crack pattern sustained by the structure at the end of the FE analysis (Fig. 7). The tensor diagrams with the maximum tensile plastic strains computed at the elements' integration points, which are presented in Fig. 7, actually illustrate crack patterns, because the direction of the vector normal to a crack plane is assumed to be parallel to the direction of the maximum principal plastic strain [7]. Thus, due to the different configurations of openings, the 4 walls have significantly different lateral strengths, but also quite different failure modes.

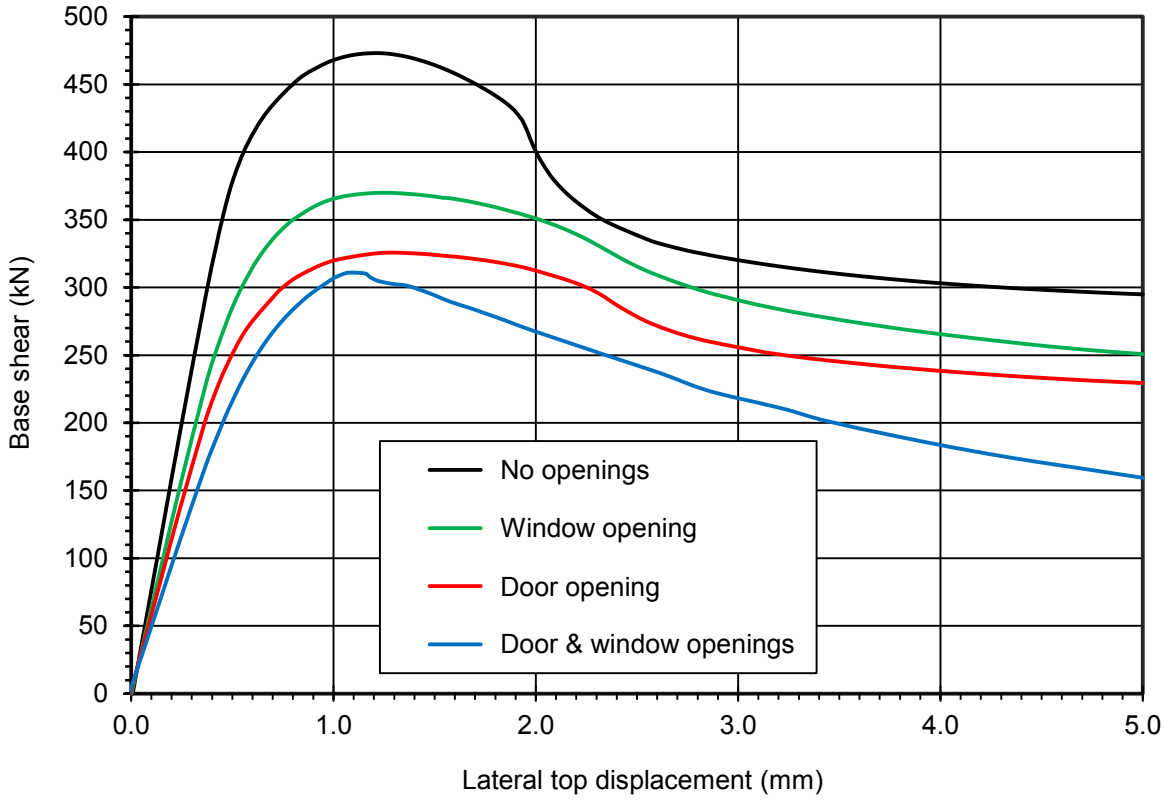

Figure 6: Force-displacement curves obtained for the 4 masonry wall configurations in their intact state (without induced base deterioration, I_{det}=0).

For the deterioration phases of Table 1, the variation of the wall's lateral strength is depicted in Fig. 8. Increasing the extent of deterioration generally leads to lower lateral strength for all 4 masonry wall configurations. However, the most significant effect is observed for the wall without openings. More specifically, compared to the intact state (I_{det}=0), the maximum deterioration phase (I_{det}=0.50) results in about 27% reduction of the maximum base shear for the wall without openings; for the walls with openings, the corresponding reductions are about 19% (window opening), 20% (door opening) and 11% (door and window openings). It is also interesting to notice that the wall with the door opening, in its intact state, is stronger that the wall with door and window openings. But, when base deterioration is induced, the wall with the two openings is stronger.

As regards the developed failure modes when base deterioration is induced, the wall without openings and the wall with the door opening actually exhibit the crack patterns of Figs 7(a) and 7(c), respectively, regardless of the adopted I_{det}-value. In the other two wall configurations, however, base deterioration changes the developed crack pattern after a certain I_{det}-value. Hence, Fig. 9 illustrates the crack pattern of the wall with window opening for I_{det}=0.50, which presents some differences compared to the crack pattern of Fig. 7(b). Moreover, Fig. 10 shows two crack patterns of the wall with door and window openings that are completely different compared to the crack pattern of Fig. 7(d). Thus, the presence of base deterioration may significantly affect not only the strength of a masonry wall, but also the cracking initiation and propagation mechanism and the ultimate failure mode.

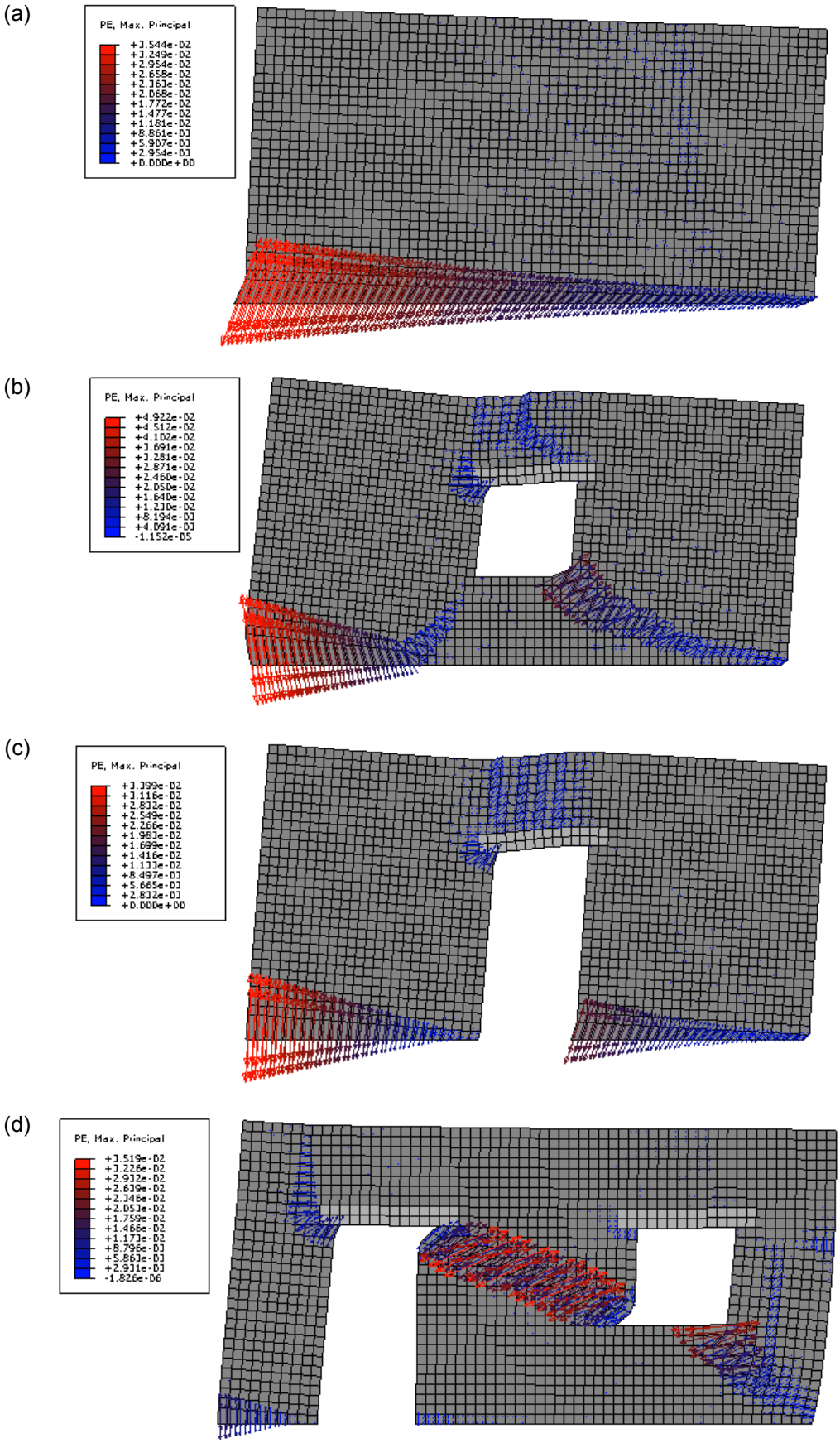

Figure 7: Deformed meshes at the final FE analysis step with tensor diagrams showing the maximum tensile plastic strains computed at the element integration points for the 4 intact masonry wall configurations (I_{det}=0).

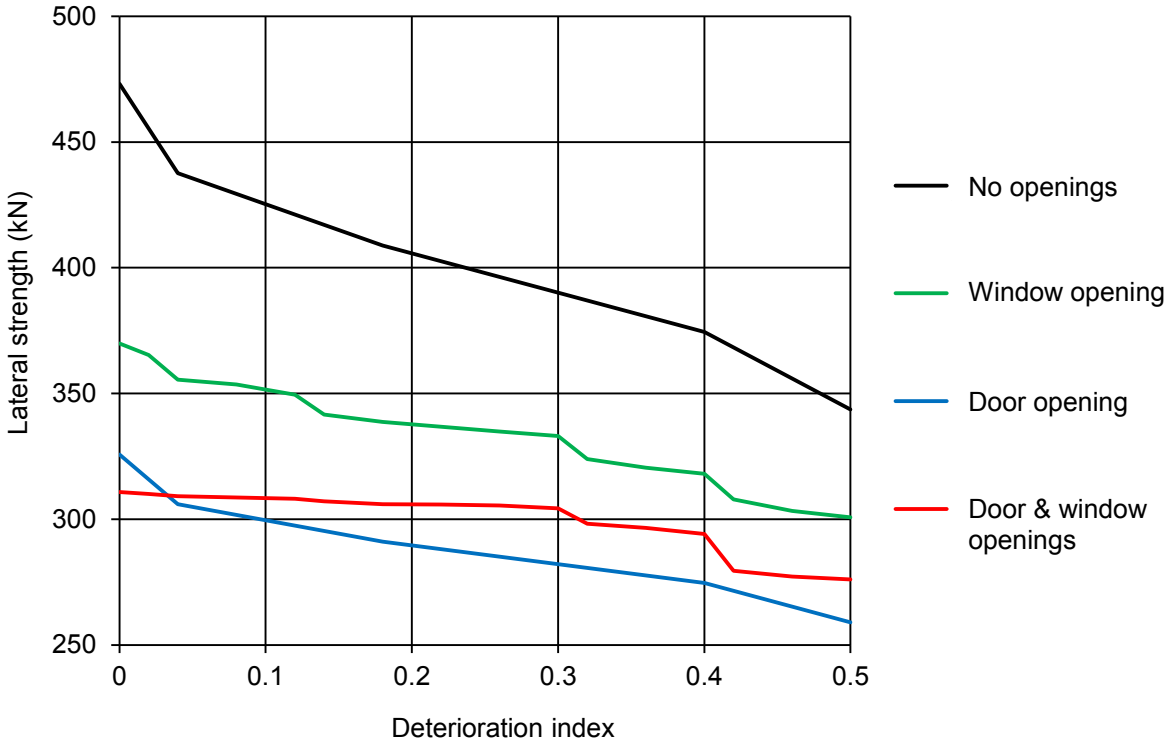

Figure 8: Lateral resistance versus deterioration index (I_{det}) relation obtained for the 4 masonry wall configurations.

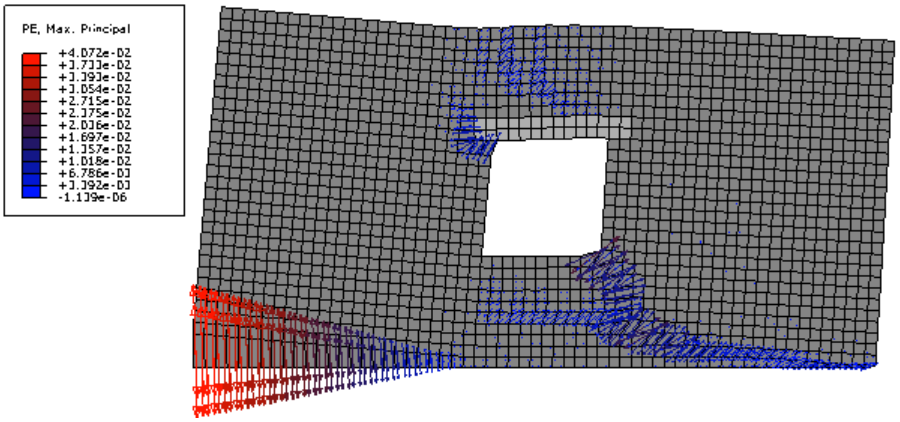

Figure 9: Deformed mesh at the final FE analysis step with tensor diagram showing the maximum tensile plastic strains computed at the element integration points for the deteriorated masonry wall with window opening (I_{det}=0.50).

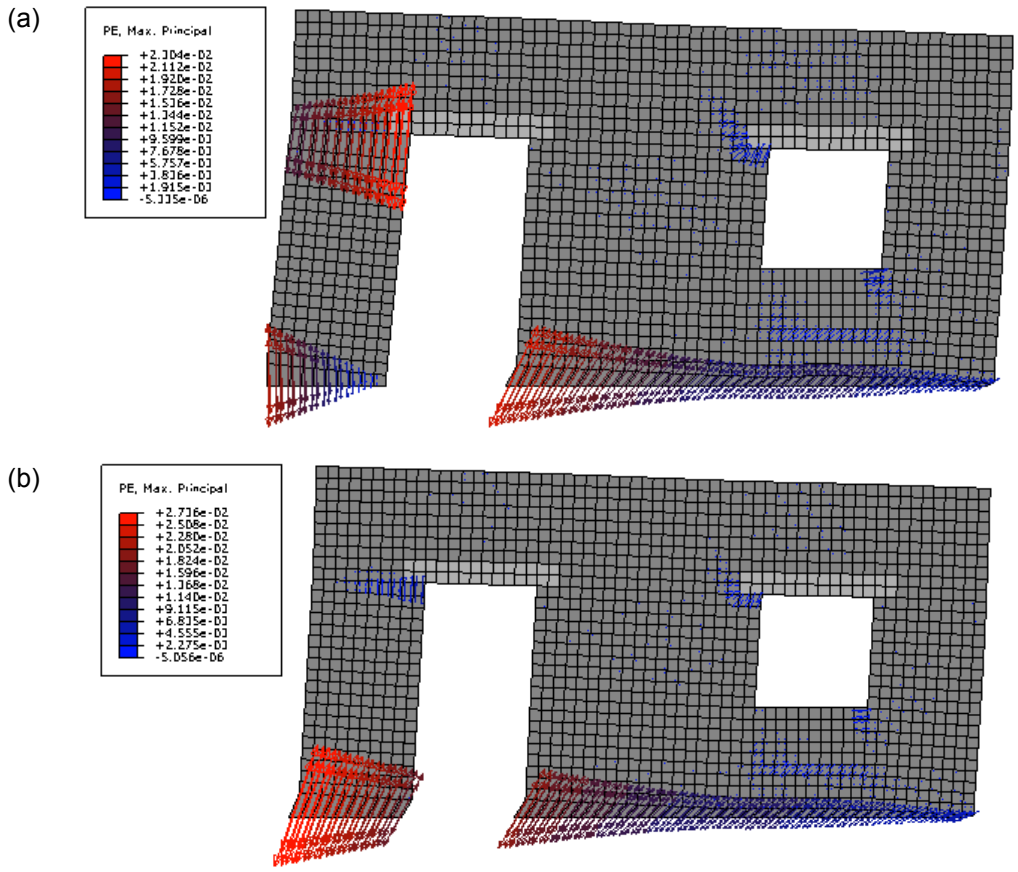

Figure 10: Deformed meshes at the final FE analysis step with tensor diagrams showing the maximum tensile plastic strains computed at the element integration points for the deteriorated masonry wall with door and window openings; (a) I_{det}=0.32, (b) I_{det}=0.50.

6 CONCLUSIONS

In this work, the aim was to numerically investigate the capability of masonry walls to sustain local damage without allowing extensive or global failure, i.e. to estimate their structural damage tolerance. More specifically, plane stress non-linear FE analyses were performed to examine the lateral in-plane strength of masonry walls under various deterioration scenarios, which were realized by notionally removing material from the base of the walls. Four wall configurations without or with window/door openings were assessed with respect to the deterioration scenarios specified. According to the obtained FE analysis results, the presence of openings and/or base deterioration in a wall result in significantly reduced lateral strength compared to an intact wall without openings. The presence of openings and/or base deterioration can also have an effect on the crack pattern developed in the wall and its eventual failure mode.

More work along the research path followed in this paper is certainly needed. It is planned to examine also masonry walls with other geometrical characteristics. In addition, the influence of the boundary conditions assumed at the foundation level could be assessed. Last but not least, future work will investigate the effect of base deterioration on the out-of-plane structural response of masonry walls damaged by base deterioration.

REFERENCES

[1] L. Binda, A. Anzani, Structural behavior and durability of stone masonry. In: *Saving our Architectural Heritage*, Chichester, Wiley, 1997.

[2] E. Doehne, C.A. Price, *Stone conservation: An overview of current research*. Getty Conservation Institute, Los Angeles, 2010.

[3] M. Steiger, A.E. Charola, K. Sterflinger, Weathering and deterioration. In: *Stone in Architecture: Properties, Durability*, Berlin, Springer, 2011.

[4] F.G. Dimes, J. Ashurst, *Conservation of building and decorative stone*. Routledge, New York, 2011.

[5] R. Illampas, I. Ioannou, D.C. Charmpis, Overview of the pathology, repair and strengthening of adobe structures. *International Journal of Architectural Heritage*, **7**, 165-188, 2013.

[6] S.J. Pantazopoulou, *State of the art report for the analysis methods for unreinforced masonry heritage structures and monuments*. OASP, Athens, 2013.

[7] Simulia Corp., *Abaqus 6.10 theory manual*. Dassault Systèmes, Rising Sun Mills, 2009.

[8] J. Lubliner, J. Oliver, S. Oller, E. Oñate, E. A plastic-damage model for concrete, *International Journal of Solids and Structures*, **25**, 299-326, 1989

[9] P. Agnihotri, V. Singhal, D.C. Rai, Effect of in-plane damage on out-of-plane strength of unreinforced masonry walls. *Engineering Structures*, **57**, 1-11, 2013.

[10] R. Illampas, D.C. Charmpis, I. Ioannou, Laboratory testing and finite element simulation of the structural response of an adobe masonry building under horizontal loading. *Engineering Structures*, **80**, 362-376, 2014.

[11] N. Mazzon, *Influence of grout injection on the dynamic behaviour of stone masonry buildings*. PhD Thesis, University of Padova, Italy, 2010.

[12] B. Silva, A. Pappas, M.R. Valluzzi, F. da Porto, C. Modena, Calibration of a material behavior model for the simulation of multi-leaf stone masonry structures: Experimental case study application. In: *Proceedings of 15th World Conference on Earthquake Engineering*, Lisbon, Portugal, 2012.

[13] S. Ganduscio, L. La Mendola, G. Zingone, Comportamento ciclico di sezioni presso inflesse in muratura. *Atti del Convegno Nazionale 'La Meccanica delle murature tra teoria e progetto'*, Messina, Italy, 1996.

[14] M. Stella, Murature in tufo calcareo: Aspetti sperimentali sulle resistenze meccaniche. *Atti del Convegno Internazionale su 'Le pietre da Costruzione in Puglia'*, Quaderno IRIS-CNR n.16, Unione Tipografica Ed., Bari, Italy, 1993.

[15] G. Marcari, G. Fabbrocino, P.B. Lourenco, Mechanical properties of tuff and calcarenite stone masonry panels under compression. In: *Proceedings of 8th International Masonry Conference*, Dresden, Germany, 2010.

[16] N. Augenti, F. Parisi, Constitutive models for tuff masonry under uniaxial compression. *Journal of Materials in Civil Engineering*, **22**, 1102-1111, 2010.

[17] R. Illampas, I. Ioannou, D.C. Charmpis, Adobe bricks under compression: experimental investigation and derivation of stress-strain equation. *Construction and Building Materials*, **53**, 83-90, 2014.

[18] P.B. Lourenço, Anisotropic softening model for masonry plates and shells. *ASCE Journal of Structural Engineering*, **126**, 1008-1016, 2000.

[19] N. Mendes, P.B. Lourenço, Comparison of different seismic non-linear analyses of an ancient masonry building. In: *Proceedings of 11th Canadian Masonry Symposium*, Toronto, Ontario, 2009.

[20] M. Dhanasekar, Review of modelling of masonry shear. *International Journal of Advances in Engineering Sciences and Applied Mathematics*, **2**, 106-118, 2010.

[21] P.B. Lourenco, *Computational strategies for masonry structures*. PhD Thesis, Faculty of Civil Engineering, Delft University of Technology, 1996.

[22] E.S. Katsaragakis, *Timber construction*. NTUA Academic Publications, Athens, 2000.

[23] D.W. Green, J.E. Winandy, D.E. Kretschman, Mechanical properties of wood. In: *Wood handbook: Wood as an engineering material*, General Technical Report FPL-GTR-113, U.S. Department of Agriculture, Forest Service, Forest Products Laboratory, Madison WI, 1999.